Japanese Journal of Radiology (2018) 36:241–256
https://doi.org/10.1007/s11604-018-0728-1

INVITED REVIEW

Pathology and images of radiation-induced hepatitis: a review article

Shigeyuki Takamatsu[1] · Kazuto Kozaka[2] · Satoshi Kobayashi[2] · Norihide Yoneda[2] · Kotaro Yoshida[2] · Dai Inoue[2] · Azusa Kitao[2] · Takahiro Ogi[2] · Tetsuya Minami[2] · Wataru Kouda[2] · Tomoyasu Kumano[1] · Nobukazu Fuwa[3] · Osamu Matsui[2] · Toshifumi Gabata[2]

Received: 13 September 2017 / Accepted: 21 February 2018 / Published online: 5 March 2018

Abstract
Recent advances in highly conformal radiotherapies greatly extend the indications for radiotherapy of liver tumors. However, because of poor tolerance to hepatic radiation, estimation of the intensity of irradiation of the liver is important, particularly for a cirrhotic liver. Knowledge of radiation-induced hepatitis is important for understanding how to optimize hepatic radiation therapy. Pathological changes of the irradiated liver, which include perivenular fibrosis, sinusoidal obstruction, and damage to Kupffer cells and hepatocytes, can be visualized using clinical imaging techniques. This review article discusses and illustrates the pathological and radiological changes of hepatic tumors and the surrounding parenchyma of the irradiated liver.

Keywords Radiation-induced liver disease · Focal liver injury · Focal liver reaction · Hepatocellular carcinoma · Pathology · Threshold dose

Introduction

Highly conformal radiotherapies such as stereotactic body radiotherapy and particle beam therapy can be safely administered. Knowledge of radiation-induced hepatitis is important for understanding how to optimize hepatic radiation therapy. Radiation-induced hepatitis is described as "radiation hepatitis", "radiation-induced hepatic toxicity", "radiation-induced liver damage", and "radiation-induced liver disease (RILD)". RILD, which describes clinical and pathological features [1–4], refers to the severity of liver toxicity after high-dose radiotherapy delivered to large liver volumes or when the whole-liver tolerance dose (30–35 Gy) is exceeded during external beam radiotherapy (RT).

RILD has become infrequent since the advent of highly conformal radiotherapy methods. Focal liver changes following application of conformal radiotherapy techniques such as stereotactic ablative body radiotherapy, stereotactic body radiotherapy (SBRT), and proton and carbon ion therapy, occur in the liver parenchyma surrounding irradiated tumors and may be symptomatic. The terms that describe post-irradiation imaging findings of computed tomography (CT) and magnetic resonance imaging (MRI) include "focal liver injury", "focal liver toxicity", "focal liver reaction", "focal liver parenchymal damage", and "focal partial liver irradiation effects" [5, 6]. There is no agreement on the terminology for describing focal hepatic changes after irradiation of the liver, and because most cases treated with highly conformal radiotherapy are inoperable, it is difficult to identify significant clinical associations of radiological findings with pathology.

Here, we use RILD to describe the effects of whole (classical) or focal (nonclassical) liver irradiation according to the original description published by Reed et al. [1]. We use "focal liver injury" to refer to focal hepatic radiation-induced changes revealed using CT and MRI. We discuss and illustrate the pathological and radiological changes of hepatic tumors and in the surrounding irradiated liver parenchyma.

✉ Shigeyuki Takamatsu
shigerad@staff.kanazawa-u.ac.jp

[1] Department of Radiotherapy, Graduate School of Medicine, Kanazawa University, 13-1 Takara-machi, Kanazawa, Ishikawa 920-8641, Japan

[2] Department of Radiology, Graduate School of Medicine, Kanazawa University, 13-1 Takara-machi, Kanazawa, Ishikawa 920-8641, Japan

[3] Department of Radiotherapy, Ise Red Cross Hospital, 1-471-2 Funae, Ise, Mie 516-8512, Japan

Table 1 Typical characteristics of hepatic radiation damage

	CLD	Fatigue	Abdominal pain	LFTs	Factors of Child–Pugh score				
					ascites	T-bil	Alb	NH_3	Plt
Classical RILD	−	+	+	ALP ↑↑ > 2 × the upper limit of normal	+	(↑)	(↓)	(↑)	(↓)
Nonclassical RILD	+	+	−	GOT/GPT ↑↑↑ 5.0–0.0 × upper limit of normal	+	↑	↓	↑	↓

RILD radiation-induced liver disease, *CLD* chronic liver disease, *LFTs* liver functional tests, *ALP* alkaline phosphatase, *GOT* glutamic-oxaloacetic transaminase, *GPT* glutamic pyruvic transaminase, *Alb* albumin, *Plt* platelet

The clinical features of radiation-induced liver disease

Post-irradiation liver damage ranges from asymptomatic conditions with or without biochemical abnormalities to fatal hepatic failure. The comprehensive term RILD includes conditions such as the different degrees of liver damage after veno-occlusive changes caused by whole or partial liver irradiation, although diagnostic criteria vary [2, 3]. Recent reports propose the separation of RILD into "classical" and "nonclassical" forms (Table 1) [4, 7, 8]. The onset of classical RILD occurs 2–12 weeks after radiation therapy and appears after the whole-liver tolerance

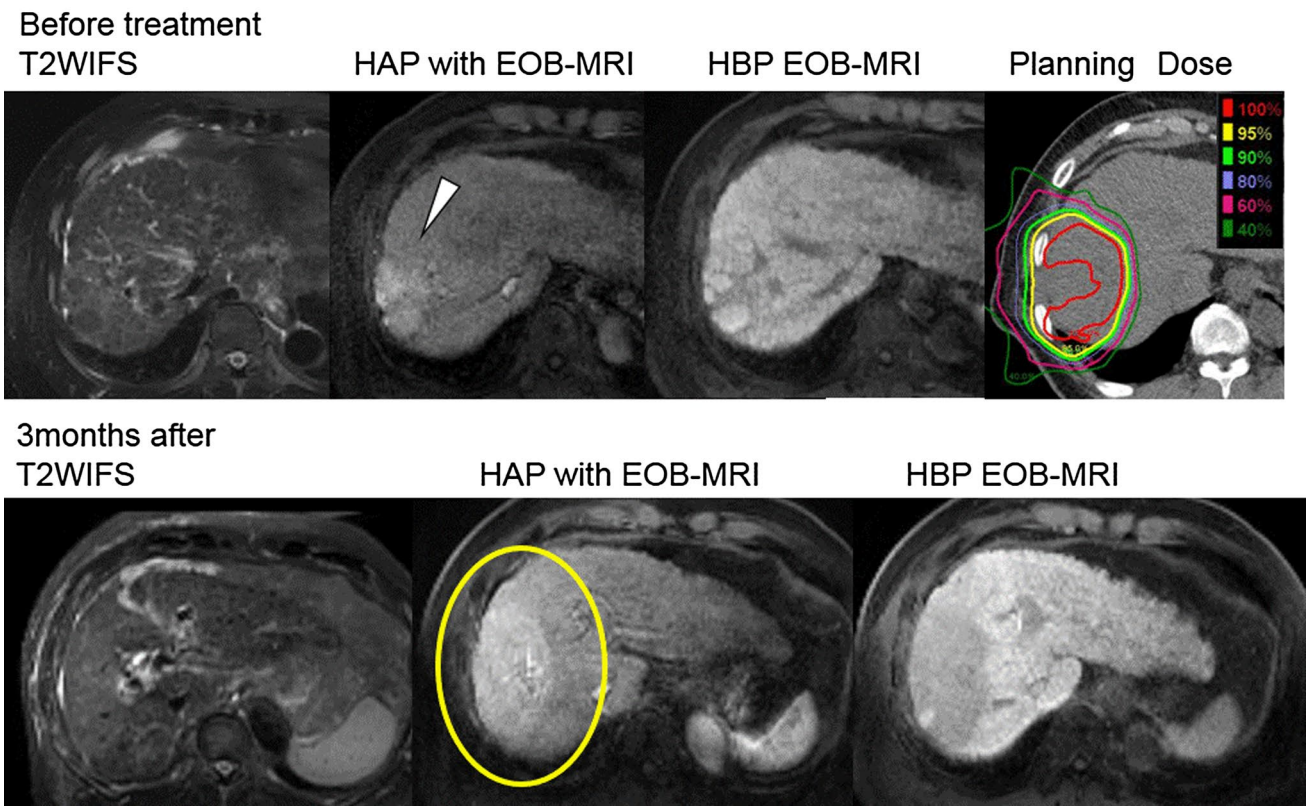

Fig. 1 S8 HCC (arrowhead) treated with PBT (76 GyE/20 Fr). During the HAP of dynamic CT before treatment, irradiated surrounding liver tissue exhibited early enhancement caused by congestive changes in the sinusoids after liver irradiation during the acute phase (circle). *T2WI* T2-weighted image, *HAP* hepatic arterial phase, *HBP* hepato-biliary phase, *HCC* hepatocellular carcinoma, *PBT* proton beam therapy, *GyE* cobalt-gray equivalent, *Fr* fractions, *HAP* hepatic arterial phase

dose (30–35 Gy) is exceeded. The hallmark of classical RILD is severe liver toxicity, accompanied by symptoms such as fatigue, abdominal pain, anicteric hepatomegaly, and ascites. An elevated level of alkaline phosphatase (> 2 × the upper limit of the normal or baseline value) is considered the most sensitive serum marker [9]. Patients with classical RILD progress to a chronic stage (liver fibrosis and failure) veno-occlusive disease (VOD) caused by radiation after 3–5 months [2, 8, 10].

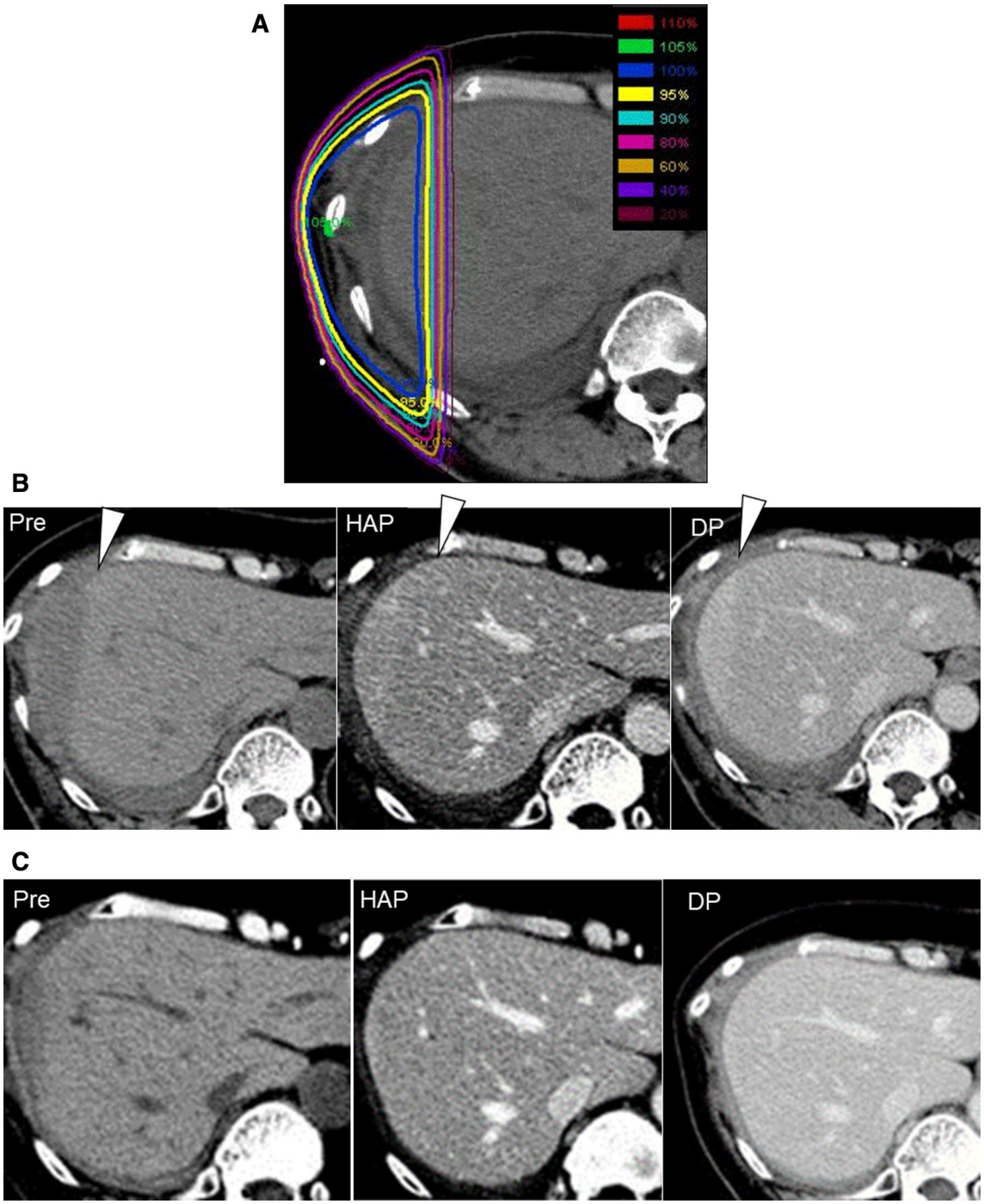

Fig. 2 Straight-border sign after X-ray irradiation (60 Gy/30 Fr/6 weeks). Dose-distribution lines for a patient with malignant mesothelioma who received postoperative radiation therapy of a pleural lesion (**a**). The straight-border sign (arrowhead) appeared at the end of treatment (**b**) and the irradiated area gradually shrank 5 months later (**c**). Scan delay for the HAP was 35-40 s, and the delayed phase (DP) was acquired 150 s after injection of the contrast enhancer. *Pre* unenhanced CT, *HAP* hepatic arterial phase, *DP* delayed phase

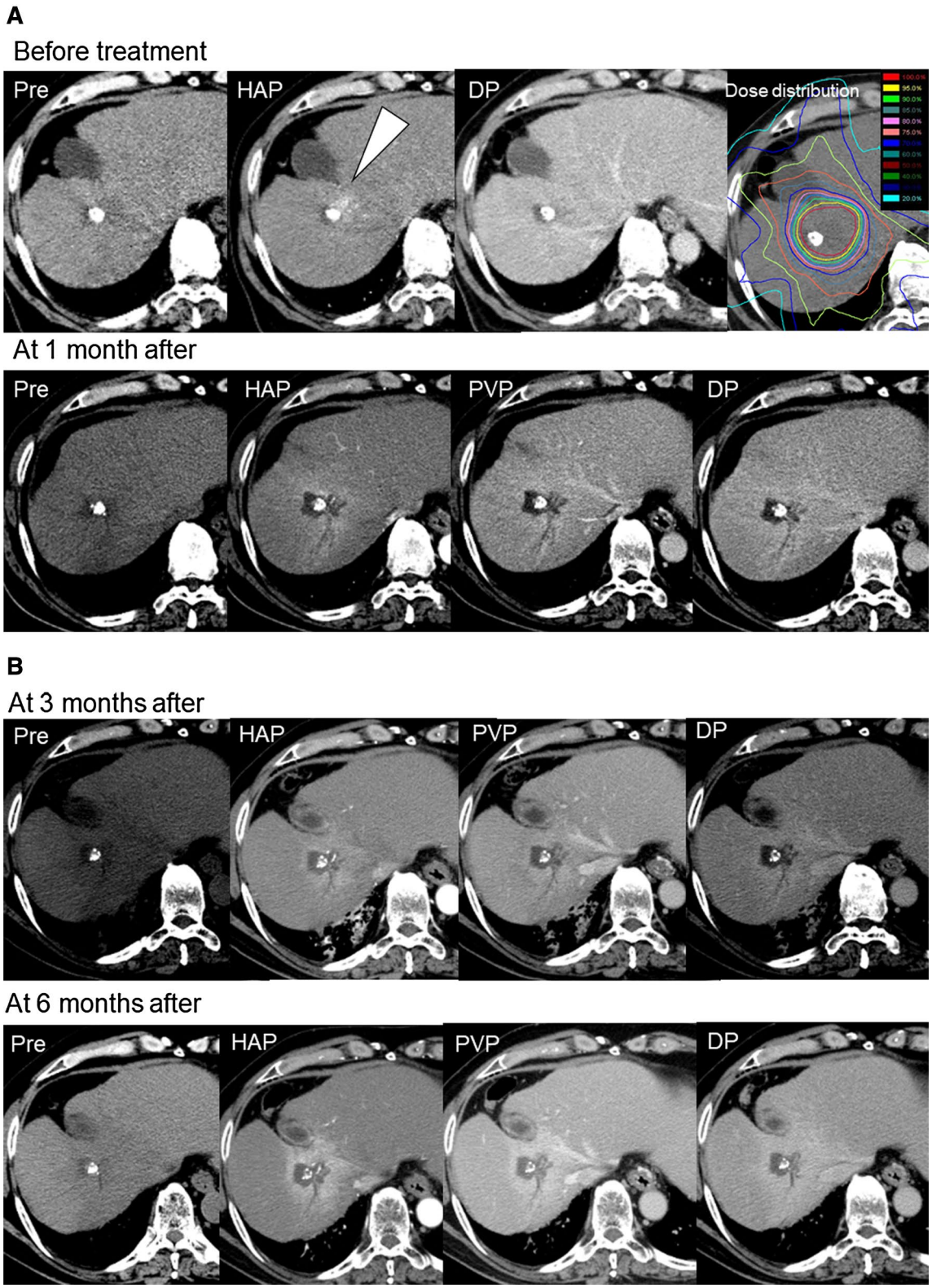

Nonclassical RILD, which is associated with the conformal RT technique, does not include the entire liver and causes focal liver damage. This serious condition is receiving attention now that whole organ irradiation is infrequently administered [7, 8, 11–13]. Most symptoms of nonclassical RILD resemble those of hepatic failure, including markedly elevated levels of serum transaminases and worsening of the Child–Pugh score (e.g., jaundice,

◂**Fig. 3** Recurrent HCC of a man in his 70 s with hepatitis C-related liver cirrhosis, Child–Pugh class A. Recurrent HCC after TACE and RFA (S8, arrowhead) was treated using SBRT (60 Gy/10 Fr). Clinical course analyzed using dynamic CT with planning dose distributions. The early enhancement of the tumor disappeared 1 month after SBRT, and focal liver injury appeared in the irradiated area (**a**). Unenhanced and enhanced CT revealed the irradiated hepatic parenchyma. In this case, type-1 findings according to Kimura's classification appeared from 1–6 months after treatment (**b**). Scan delays for HAP and PVP were 35–40 and 70 s, respectively. The DP was imaged 150 s after injection of the contrast medium. *Pre* unenhanced CT, *HAP* hepatic arterial phase, *PVP* portal venous phase, *DP* delayed phase, *HCC* hepatocellular carcinoma, *TACE* transcatheter arterial chemoembolization, *RFA* radiofrequency ablation, *SBRT* stereotactic body radiotherapy

ascites). Morbidity depends on the extent of preexisting hepatic pathology. During the clinical course of patients with chronic liver disease, the onset of nonclassical RILD occurs 1–12 weeks after radiation therapy [5, 6].

The clinical utility of the diagnosis of nonclassical RILD and its underlying pathology is poorly understood. Efforts to generate a scoring system for nonclassical RILD according to the National Cancer Institute Common Terminology Criteria for Adverse Events (CTCAE) [14] include the introduction of the variables as follows: (1) Elevated levels of liver transaminases (greater than CTCAE Gr. 3) of patients with normal baseline values or greater than CTCAE Gr. 4 levels in patients with baseline values greater than CTCAE Gr. 3. (2) Decline in liver function (worsening of Child–Pugh class ≥ 2) in the absence of classical RILD [7, 11]. Sanuki et al. define three clinically relevant events that affect overall survival of patients with hepatocellular carcinoma (HCC) if they occur within 12 months after administration of SBRT as follows: (1) Elevated liver transaminase levels (CTCAE Gr. 3) within 3 months of completion of RT. (2) Thrombocytopenia (CTCAE Gr. 3). (3) Worsening of the Child–Pugh score to > 8) [7]. CT and MRI of focally irradiated liver can identify focal hepatic changes. Some cases of focal liver injury after highly conformal irradiation worsen to nonclassical RILD. To avoid misdiagnosis, radiologists should, therefore, become familiar with the imaging features of focal liver injury caused by liver irradiation and possible mimics (Figs. 1, 2, 3) [5, 6].

The pathological changes in irradiated liver

The pathological changes in irradiated liver can be approximately divided into acute (1–3 months), subacute (3–6 months), and chronic (> 6 months) phases. In the acute phase, massive portal and systemic venous congestion, fibrin thrombi within sinusoids, perisinusoidal hemorrhages, reactive hyperemia, atrophy, and degeneration of hepatocytes are widely observed around the centrilobular areas of hepatic acinus, the so-called zone III. In this phase, Kupffer cells exhibit radiation damage. In the subacute phase, obstruction of sublobular veins is superimposed upon the acute-phase findings. In the chronic phase, moderate elastosis in the walls of the central veins and mild elastosis in the walls of perivenular sinusoids cause occlusion of the central veins because of fibrosis, lobular collapse and distortion, and accumulation of Kupffer cells, occasionally with deposition of hemosiderin [2, 3, 5, 6].

The main pathological changes in the irradiated liver are congestion caused by obstruction of hepatic venous outflow through a combination of endothelial cell edema, terminal hepatic venule narrowing, sinusoidal congestion, zonal parenchymal atrophy, and accumulation of collagen in the subendothelial space (space of Disse). These events predominate around zone III, and the histopathological features are similar to those of VOD induced by causes (e.g., high-dose chemotherapy, viral infection), including occlusive fibrosis of intrahepatic veins, congestion with extravasation of red blood cells, and alternating areas of hepatocyte atrophy and regeneration (Fig. 4) [1].

Radiation that damages the subendothelial basement membrane leads to activation and aggregation of platelets and stimulates dormant hepatic stellate cells [3, 4]. Damage to the hepatic venule endothelium contributes to the formation of microthrombi that cause venous obstruction, panlobular congestion, hepatocyte loss, and fibrosis mediated by transforming growth factor-β1 (TGF-β1) [15–18]. In animal studies, TGF-β1 levels increases in irradiated dose dependent and it was significantly correlated with the fibrosis [17, 18]. Further, radiation damage to Kupffer cells is important to consider when we evaluate the findings of superparamagnetic iron oxide (SPIO) MRI of the patients who undergo radiotherapy. The radiosensitivity of these specialized macrophages is higher compared with that of the hepatocyte [19].

CT and MRI imaging of RILD and focal liver injury

CT imaging

Whole-liver irradiation causes classical RILD, characterized by anicteric hepatomegaly and ascites without jaundice. CT imaging shows low periportal attenuation with or without enhancement and contrast-enhanced CT reveals heterogenous liver enhancement caused by liver congestion [20, 21].

After focal irradiation of the liver, the irradiated hepatic parenchyma, compared with the surrounding nonirradiated hepatic parenchyma, typically shows hypoattenuation on

unenhanced CT and hyperattenuation on contrast-enhanced CT, with nonanatomical distribution secondary to focal congestive and fibrotic changes characteristic of focal liver injury.

Considering the relationship between pathological changes and imaging findings, the cause of hypoattenuation on unenhanced CT is attributable to hepatic edema or congestion caused by pathologically focal VOD-related changes, fibrotic changes, hemorrhagic or necrotic changes or both. Radiotherapy causes venous occlusion and hepatic fibrosis, which change hepatic hemodynamics because of occluded venous drainage and decreased portal-vein inflow with compensating increased arterial inflow. Therefore, the abnormal early enhancement of the irradiated liver occurs during the arterial phase of dynamic CT and MRI.

The outflow obstruction caused by VOD, revealed by abnormal arterial enhancement, is followed by a heterogeneous portal venous phase and delayed-phase enhancement caused by the concentration of contrast media in dilated hepatic sinusoids and the retention of contrast media in the interstitium of hypertrophied fibrous tissue, particularly during the delayed phase [22]. Further, there is delayed washout of contrast from fibrotic tissue. These factors explain why the irradiated parenchyma shows prolonged enhancement throughout the dynamic phases.

When nonconformal radiotherapy is administered to the liver, the borders of the altered attenuation areas are straight and their distributions are not anatomic. This is called a "straight-border sign" (Fig. 2). There are other causes of the straight-border sign, such as vascular

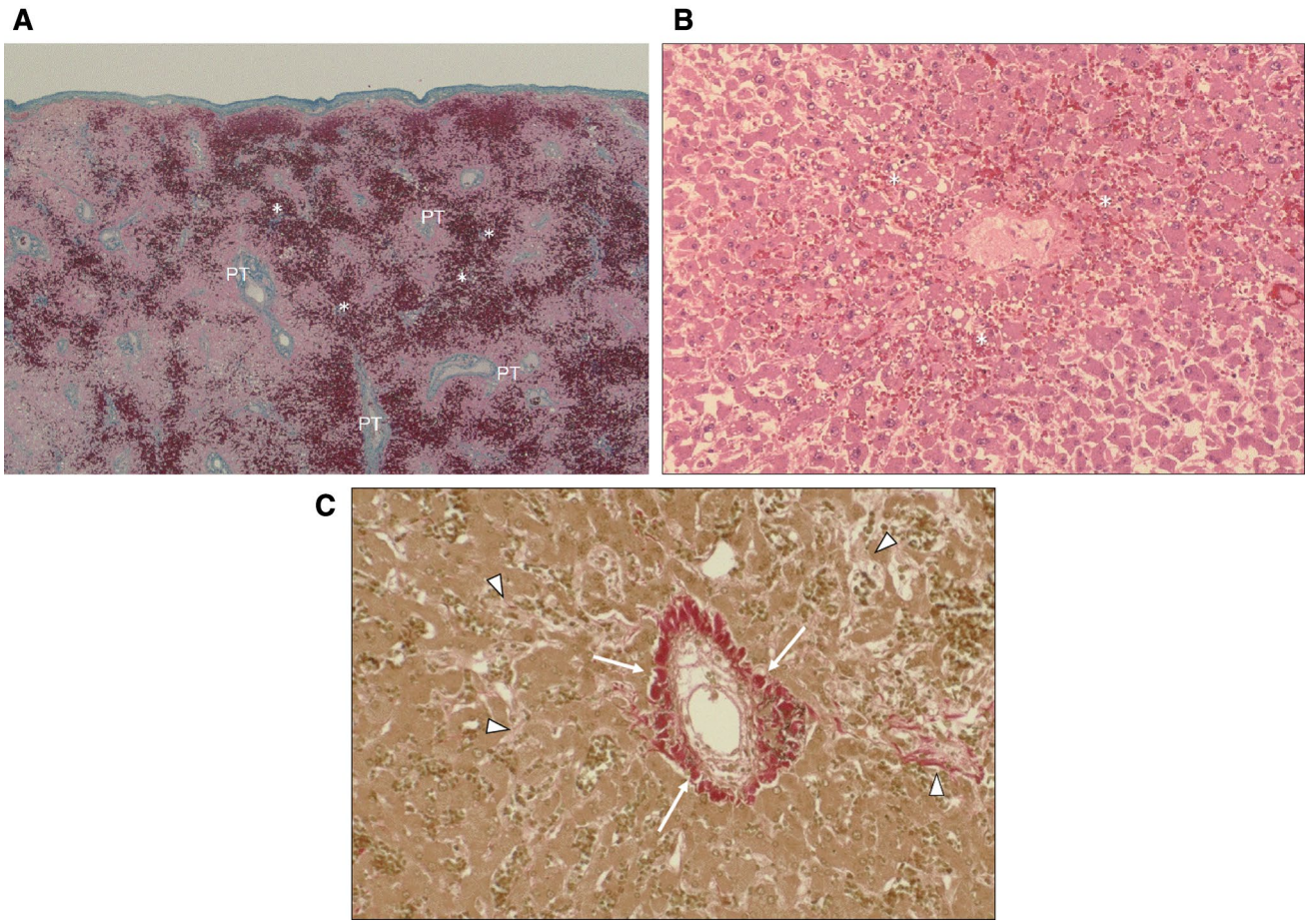

Fig. 4 Pathological specimens of patients with hepatic VOD after liver irradiation. **a** A patient with lower intrathoracic esophageal cancer 10 days after completing curative chemoradiotherapy (88.4 Gy/52 fractions/112 treatments. Loupe image of azan stain showing massive hepatic congestion around the centrilobular area (zone III, asterisk). **b**, **c** A patient with lung cancer in the left lower lobe 25 days after completion of chemoradiotherapy (40 Gy/20 fractions). Dilated hepatic sinusoids and aggregation of red blood cells (**b**, asterisk) are located in the centrilobular area [**b**, magnification (×100) of the centrilobular area stained with hematoxylin and eosin]. Moderate elastosis in the wall of the central vein (**c**, arrow) and sinusoidal dilatation and mild elastosis in the walls of perivenular sinusoids (**c**, arrowhead), reflecting panlobular congestion (**c**, magnification [×100] of the centrilobular area stained using Elastic von Gieson stain). Histopathological features of the radiation-induced liver disease are indistinguishable from those of VOD caused by other pathologies. *VOD* veno-occlusive disease, *PT* portal tract

obstruction, arterioportal shunt, focal fatty infiltration, and confluent hepatic fibrosis [21, 23]; however, they conform to an anatomical distribution. However, a pseudoanatomic distribution is occasionally observed after rectangular, two-port irradiation using a wedge device or proton beam irradiation (Fig. 1). Reference to planning dose-distribution lines will help correctly diagnose focal liver injury (Figs. 1, 5, 6, 7). The irradiated liver gradually shrinks; the surrounding liver parenchyma not exposed to radiation undergoes compensatory hypertrophy, particularly in the chronic phase [24], and displays normal (lower) enhancement.

According to Kimura et al. [25], the dynamic CT enhancement pattern after focal liver irradiation can be classified into the patterns as follows: Type 1, hyperdensity in all enhanced phases, which is observed in otherwise normal irradiated liver; Type 2, hypodensity in the arterial and portal venous phases; and Type 3, isodensity in all enhanced phases. Kimura et al. [25] further reported that the majority of subjects exhibited Type 1. Half of Types 2 and 3 subjects (Child–Pugh class A) reverted to Type 1. After 3–6 months, Child–Pugh class B was a significant predictor of a Type 3 appearance. In most patients with Child–Pugh class A, the dynamic enhancement pattern significantly reverted to Type 1 (Figs. 3, 6), remaining stable for ≥ 1 year. These features most likely reflect the pathological changes after irradiation as a function of the severity and reversibility of the baseline pathology of the liver, such as the degree of hemodynamic alteration, hepatic fibrosis, and inflammation.

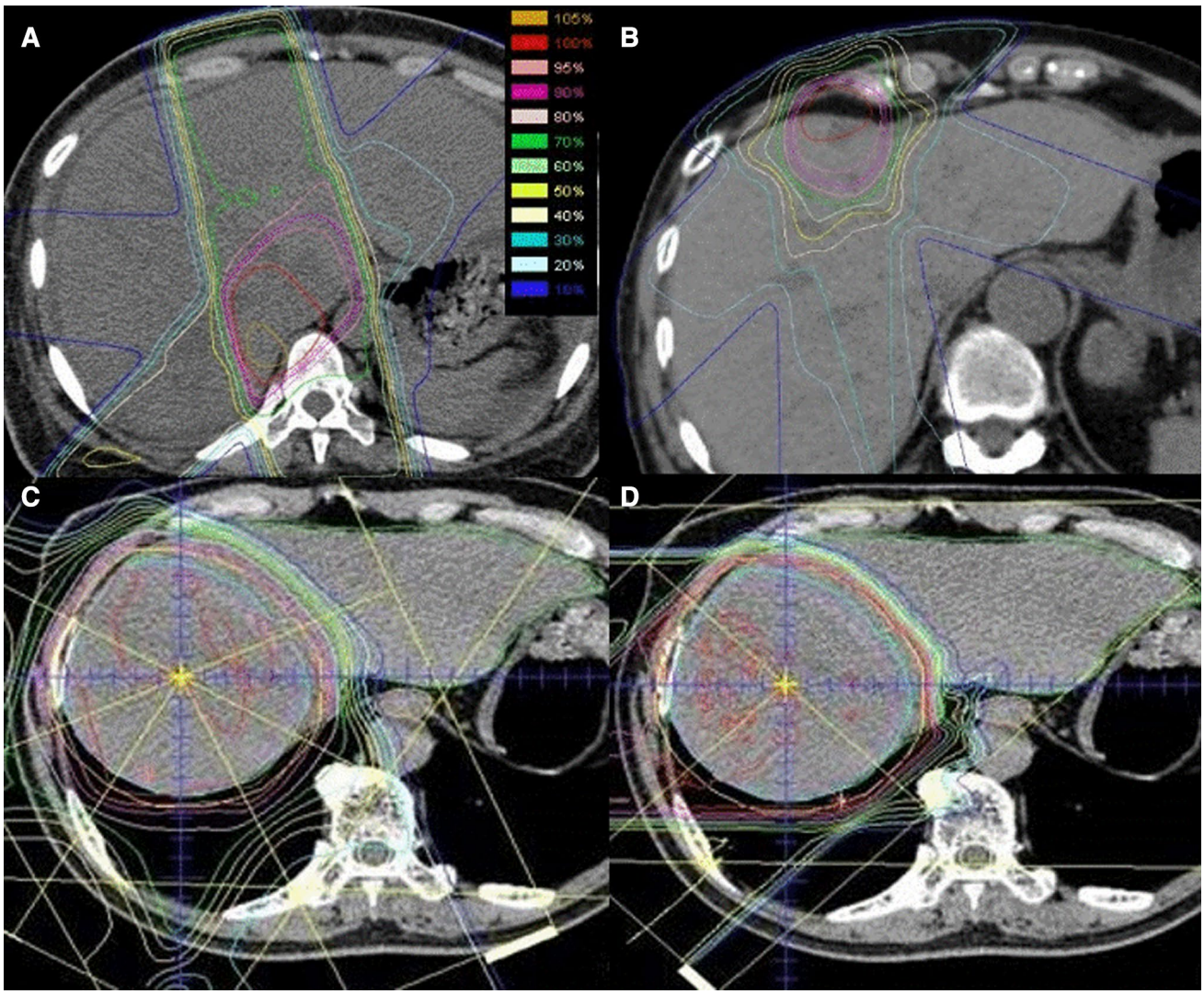

Fig. 5 Dose-distribution lines of different radiotherapy techniques: conventional external beam radiation therapy (**a**), stereotactic body radiotherapy (**b**), proton beam therapy (**c**), and carbon ion therapy (**d**). In conformal radiotherapy such as SBRT or particle beam therapy, a straight border is not always present. To diagnose focal liver injury, it is important to refer to the radiation dose-distribution images. *SBRT* stereotactic body radiotherapy

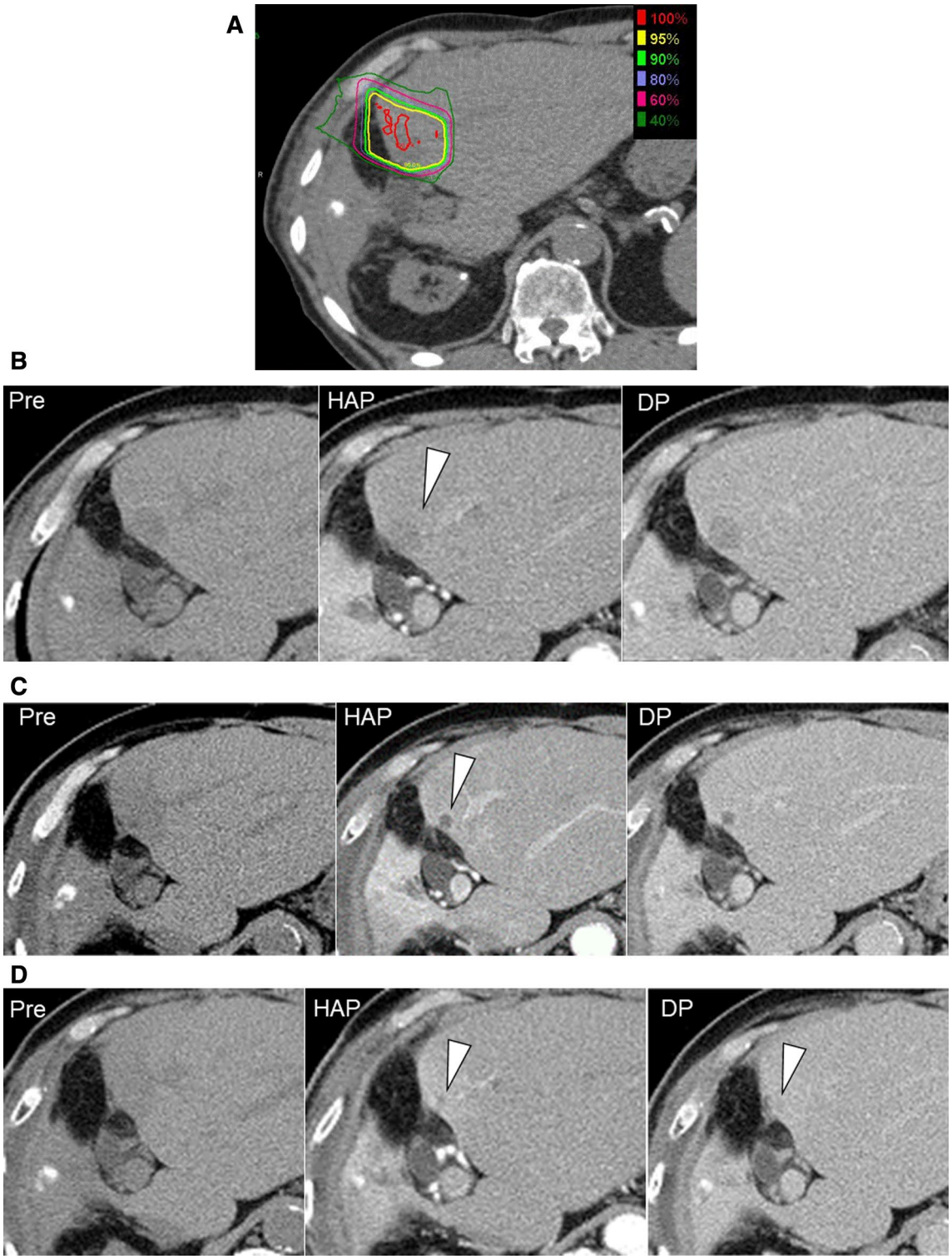

Fig. 6 CT images of focal liver injury after PBT for HCC. A man in his 70 s with hepatitis C-related liver cirrhosis, Child–Pugh A, with hypervascular HCC (S3, arrowhead) treated using PBT (66 GyE/10 Fr) (**a**). Contrast-enhanced CT images before treatment (**b**), 3 months after (**c**), and 6 months after (**d**). Using Kimura's Classification, type 3 findings appeared 3 months after treatment (**c**), changing to type 1 at 6 months (**d**). Scan delay for the HAP was 35–40 s and the DP was acquired 150 s after injection of the contrast medium. *Pre* unenhanced CT, *HAP* hepatic arterial phase, *DP* delayed phase, *PBT* proton beam therapy, *HCC* hepatocellular carcinoma, *GyE* cobalt-gray equivalent, *Fr* fractions

MRI of RILD and focal liver injury

MRI analysis of Classical RILD reveals the same findings as CT, which includes anicteric hepatomegaly, ascites, and liver congestion. Further, periportal edema is revealed by hyperintensity in T2-weighted images (T2WIs) and heterogenous liver enhancement with enhanced contrast because of liver congestion.

After focal liver irradiation, MRI visualizes focal liver injury using various sequences (Figs. 1, 7, 8). The straight-border sign of conventional radiotherapy, the border between the irradiated and nonirradiated liver can again be distinguished, and the conformal radiotherapy techniques identify their targets as rounded focal shapes. To diagnose focal liver injury, it is important to refer to the radiation dose-distribution images (Fig. 5). In areas of focal edema or congestion caused by VOD and hepatic fibrosis, irradiated liver parenchyma typically exhibits a sharply defined wide band of hypointensity on T1-weighted images (T1WI), hyperintensity on T2WIs, slight hyperintensity on diffusion-weighted imaging (DWI), and low apparent diffusion coefficient (ADC) values correspond to the radiation port [26–28]. Dynamic contrast-enhanced MRI often reveals early straight-border enhancement persisting into the delayed phase, similar to dynamic CT (Figs. 1, 7) [21,

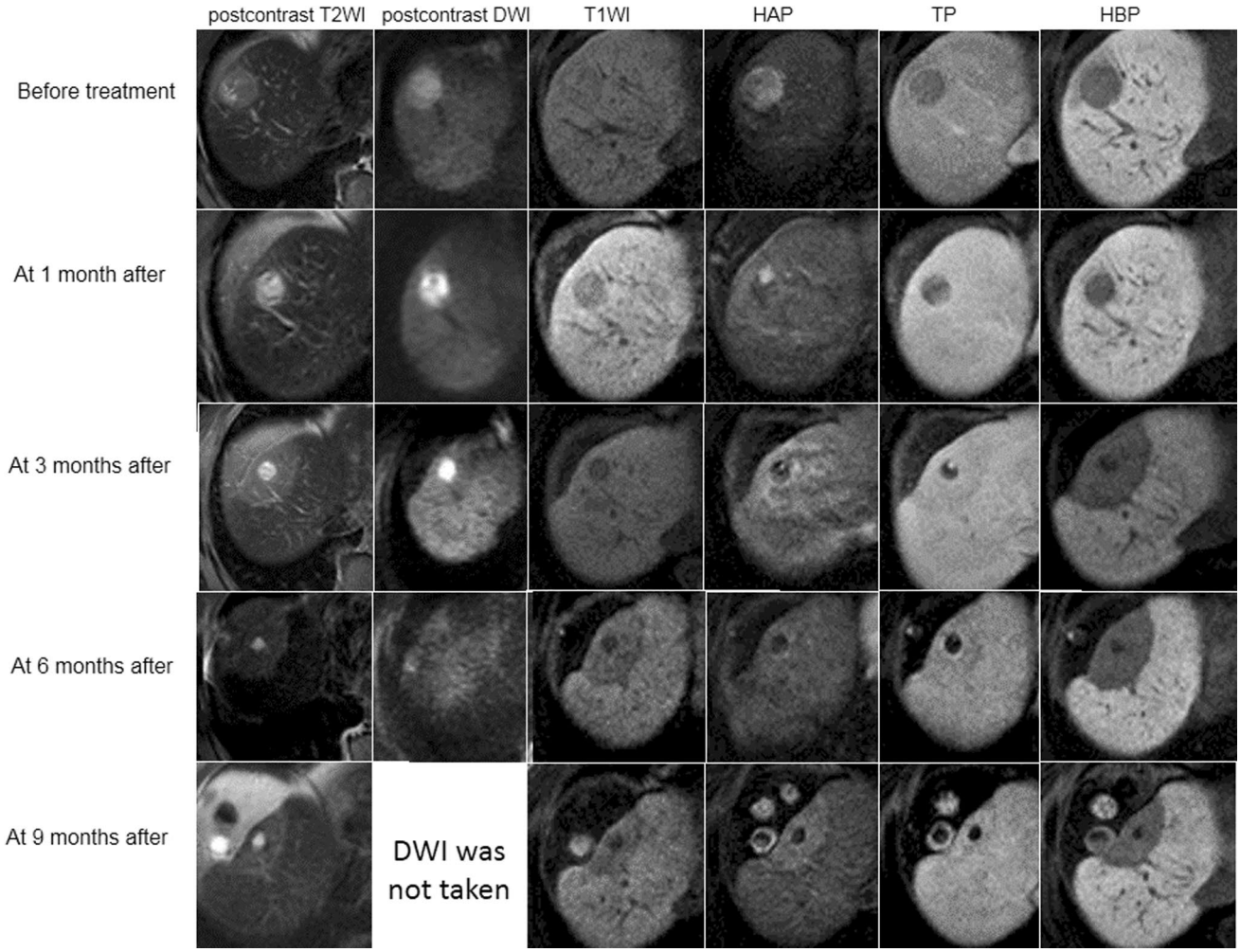

Fig. 7 A patient with nonalcoholic steatohepatitis, Child–Pugh class 5, with a 30-mm HCC in S8 who underwent PBT (66 GyE/10 Fr). Imaging of irradiated liver using different sequences of dynamic EOB-MRI at treatment planning. Focal liver injury was apparent 3 months after treatment, demonstrated by a well-defined band of hyperintensity on T2WI (**a**) and hypointensity on T1WI (**c**) of the irradiated liver, corresponding to the radiation port. The area undergoing arterial enhancement (**d**), which decreased in size after PBT, was observed as a sharp hypointense border between the irradiated and nonirradiated areas as **a** during the HBP of EOB-MRI (**f**). The area of HCC was hypointense in the DWI (**b**), suggesting the absence of viable HCC cells. The size of the focal area of the injured liver decreased and the decrease in the volume of the focal liver injury volume is revealed in this series of follow-up MRI images. *HCC* hepatocellular carcinoma, *PBT* proton beam therapy, *GyE* cobalt-gray equivalent, *Fr* fractions, *T2WI* T2-weighted image, *DWI* diffusion-weighted image, *T1WI* T1-weighted image, *HBP* hepato-biliary phase

22]. These findings reflect the pathological changes of acute, subacute, and chronic disease phases.

The most sensitive technique that can visualize early phase focal liver injury may be SPIO-MRI [19]. Damage to Kupffer cells is accompanied by a functional decrease in their phagocytic capacity for SPIO. Decreased SPIO uptake appears as hyperintensity on long echo-time gradient images (Fig. 8). Although its use is currently limited to the detection of hepatocellular carcinoma [29], SPIO imaging can visualize focal liver injury earlier than hepatocyte-specific gadolinium agents such as gadoxetate disodium (gadolinium ethoxybenzyl diethylenetriamine pentaacetic acid [Gd-EOB-DTPA]) and gadobenate disodium (gadobenate dimeglumine [Gd-BOPTA]) [30], which are widely used to identify HCCs and liver metastases [31, 32].

Gd-EOB-DTPA is mainly incorporated into hepatocytes by organic anion transporting polypeptide (OATP) 1B3 and its uptake rate significantly correlates with OATP1B3 expression in normal hepatocytes and HCC cells [33, 34]. OATP1B3 is predominantly expressed in hepatocytes distributed around zone III in normal liver parenchyma [35]. Because a major histopathological change in radiation-induced liver damage predominantly occurs in zone III, the hepato-biliary phases (HBPs) of Gd-EOB-DTPA-enhanced MRI (EOB-MRI) can demonstrate focal liver injury as a defined hypointense area 3 months after irradiation (Fig. 7) [24].

Other reasons that explain why the hypointensity of irradiated parenchyma detected using EOB-MRI to analyze the HBPs include direct damage to hepatocytes, inhibition of the expression of the OATP1B3 receptor, and inhibition of Gd-EOB-DTPA transport by the accumulation of collagen in the subendothelial space (space of Disse). Moreover, hepatocytes as well as Kupffer cells and sinusoidal endothelial cells play key roles in reducing the signal intensity of EOB-MRI. The cytokines released by these cells influence the decrease of the Gd-EOB-DTPA uptake by transporter proteins in the irradiated parenchyma, thereby decreasing hepatocyte-specific Gd-EOB-DTPA uptake [36].

Likelihood of RILD after radiation therapy

The prediction of the likelihood of RILD is clinically important for patients who undergo liver irradiation. The liver is a redundant organ, comprising multiple functional subunits (hepatic lobules) capable of regeneration that allow a part of the liver to be sacrificed without loss of function. Various

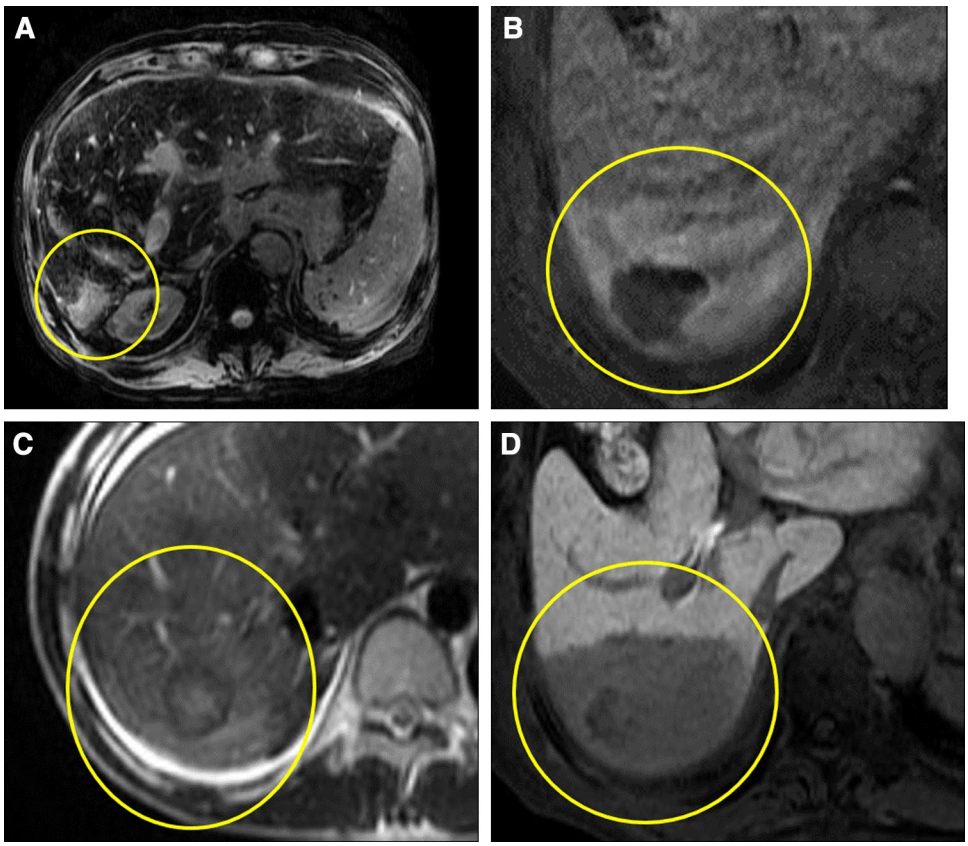

Fig. 8 Each sequence in the MR imaging shows RILD. SPIO-MRI long TE image (**a**), HAP with dynamic Gd-EOB-DTPA enhancement (**b**), T2WI (**c**), HBP with Gd-EOB-DTPA (**d**). The focal liver injury can be visualized on MRI using various sequences. *RILD* radiation-induced liver disease, *SPIO* super paramagnetic iron oxide, *HAP* hepatic arterial phase, *HBP* hepato-biliary phase

approaches and models, which are available for predicting RILD, use radiation doses as variables in a mathematical model, for example, the Lyman–Kutcher–Burman normal tissue complication probability model [37–39]. Others use clinical and dosimetric variables as in the logistic regression model [40], an artificial neural network model [41], and dose-volume histogram analysis as in the Quantitative Analyses of Normal Tissue Effects in the Clinic (QUANTEC) review [42, 43].

These theories are applied to a patient's clinical background and the planning data for each treatment strategy. For example, in the QUANTEC review, the liver tolerance doses are divided according to a diagnosis of primary cancer arising in a liver with chronic liver disease vs metastasis arising in an otherwise normal liver [42, 43]. The QUANTEC study separated patients undergoing whole vs focal liver irradiation. The important factors for predicting RILD are whole-liver radiation dose, background hepatic reserve, mean normal liver dose, and normal liver volume (less than the threshold dose) [42, 43].

The analysis of residual liver volume after resection is important and formulas are available that predict the standard liver volume [44, 45]. For example, the percentage volume of nonirradiated normal liver is significantly related to liver function after proton beam therapy [46]. However, no formula calculates the residual liver volume after radiotherapy. If the focal hepatic changes in CT or MRI accurately shows damaged liver as a loss of functional area, determining the threshold doses of these changes may be clinically important for calculating residual liver volume before radiation therapy to provide a preliminary estimate of residual liver volume before hepatectomy for HCC or liver metastases [2, 47–50].

Nakamura et al. reported a useful prediction parameter for irradiated liver using EOB-MRI for SBRT of HCC. Briefly, their original parameter, weighted liver-spleen contrast for each radiation dose area for the HBP of EOB-MRI, is useful for predicting changes in hepatic function after SBRT, independent of standard parameters, which are calculated according to the mean liver dose and the percentage of the liver volume exposed to > 20 Gy [51].

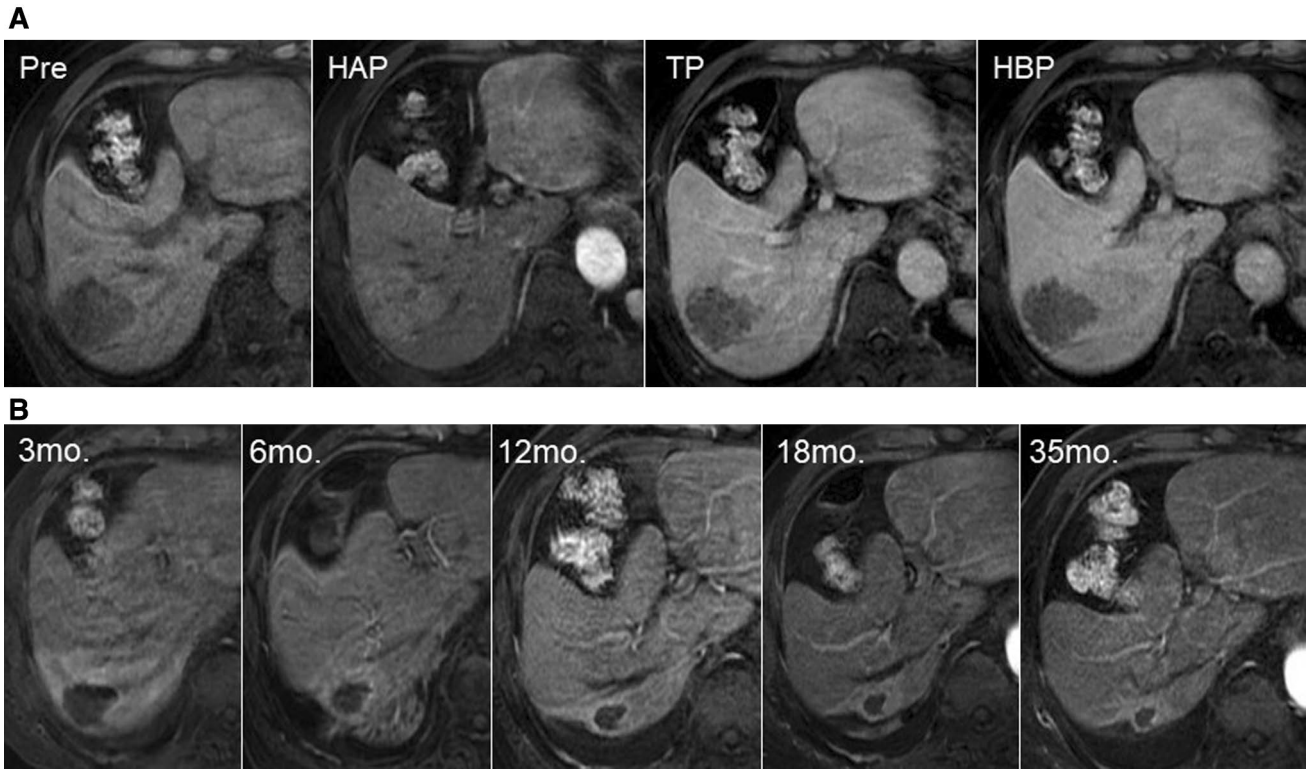

Fig. 9 Enhanced dynamic imaging of irradiated HCC and liver using Gd-EOB-DTPA. HCC (S5/6) treated using PBT 66 GyE/10 Fr before treatment (**a**). HAP at each follow-up period (**b**). HCC without early enhancement during the arterial phase. Volume reduction of the HCC and surrounding focal liver injury. *Pre* unenhanced CT, *HAP* hepatic arterial phase, *TP* transitional phase, *HBP* hepato-biliary phase, *mo* months, *HCC* hepatocellular carcinoma, *PBT* proton beam therapy, *GyE* cobalt-gray equivalent, *Fr* fractions

Evaluation of the response of HCC after radiotherapy

It is important to evaluate the therapeutic response to malignant tumors after radiation therapy, although assessment can be challenging. T1WI and T2WI images of recurrent tumors and the irradiated areas show similar characteristics. Most residual masses show hypointensity during the HBP of EOB-MRI and it is difficult to distinguish them from the surrounding irradiated liver. In Gd-DTPA-enhanced dynamic MRI, recurrent HCC typically shows early enhancement, followed by a rapid washout (Figs. 9, 10, 11) [52]. However,

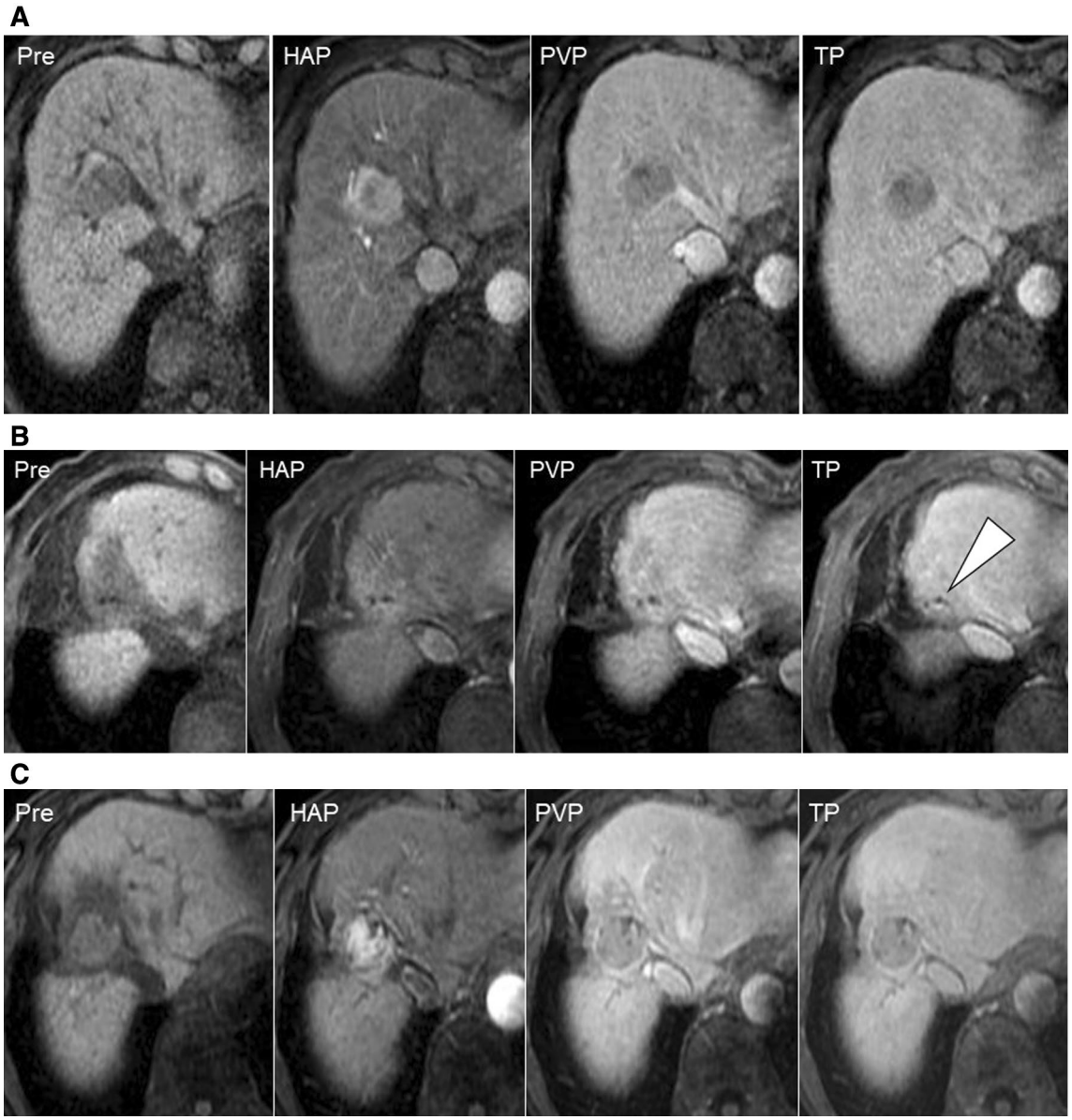

Fig. 10 A man with HCC in his 70 s with hepatitis B-related liver cirrhosis, Child–Pugh class A, treated using PBT (66 GyE/10 Fr). Dynamic EOB-MRI images before treatment (**a**) and after treatment after 17 (**b**) and 27 months (**c**) show progression of the recurrent HCC after PBT. An irradiated HCC exhibiting a scar-like appearance that was hypointense during unenhanced and all enhancement phases (**b**, arrowhead). The focal liver injury surrounding the scar-like HCC area was hypointense in precontrast images, hyperintense during the HAP, hypointense during the PVP, and isointense during the TP (**b**). Focal liver injury surrounding a recurrent HCC (**c**) was hypointense in precontrast T1WIs and was locally controlled at 17 months, although regrowth of the tumor appeared after 27 months (**c**). Salvage TACE + RFA was administered and provided local tumor control for 8 months until death. Scan delay of the HAP was 20–35 and 70–90 s for the PVP. DP was acquired 4–5 min after injection of the contrast medium. *Pre* unenhanced CT, *HAP* hepatic arterial phase, *PVP* portal venous phase, *TP* transitional phase, *HCC* hepatocellular carcinoma, *PBT* proton beam therapy, *TACE* transcatheter arterial chemoembolization, *RFA* radiofrequency ablation

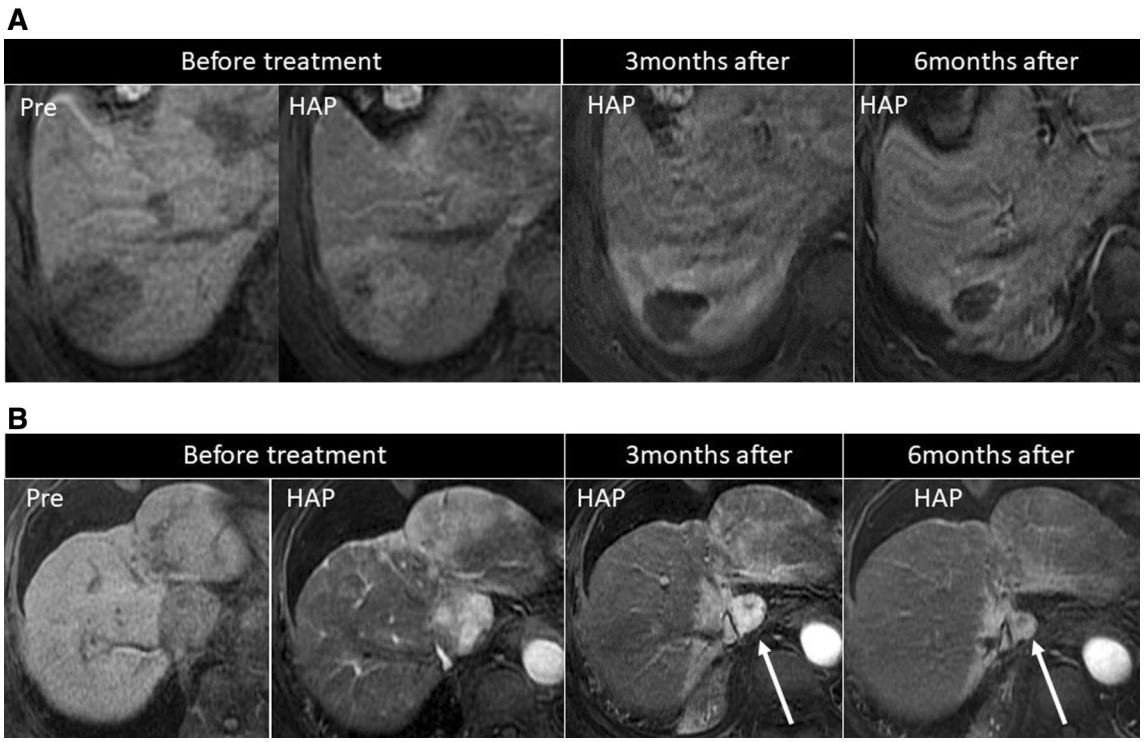

Fig. 11 Changes in arterial staining after treatment of HCC. Tumor regression with (**a** case 1) and without (**b** case 2, arrow) disappearance of tumor staining. Tumor regression and the disappearance of tumor staining are useful for the estimation of therapeutic effects. However, some HCCs gradually become smaller without disappearance of early staining. In these two cases, HCC was locally controlled longer than 3 years after PBT. Some HCCs exhibit arterial enhancement after radiotherapy and the irradiated surrounding liver typically shows early enhancement. These findings are confusing and can be misdiagnosed as recurrent HCC. *HAP* hepatic arterial phase, *HBP* hepato-biliary phase, *HCC* hepatocellular carcinoma, *PBT* proton beam therapy

the irradiated liver parenchyma shows early enhancement and contrast enhancement tends to be more prominent and prolonged, as discussed in the section on CT and MRI imaging of RILD and focal liver injury. Thus, radiologists should be aware that the early stain of residual HCC may be masked in the early enhancement of the surrounding hepatic parenchyma. Characteristic findings revealed by the time-intensity curve of a dynamic MRI study with contrast enhancement provide clues that distinguish recurrent HCC from radiation-induced hepatic injury [52].

Table 2 Estimation of the therapeutic effect on HCC according to response evaluation criteria

	Case 1		Case 2	
	At 3 months	At 6 months	At 3 months	At 6 months
RECIST	PR	PR	PR	PR
m-RECIST	CR	CR	PR	PR
EASL	CR	CR	PR	PR
RECICL	TE4(CR)	TE4(CR)	TE3(PR)	TE3(PR)

Tumor regression shown in Fig. 11 without (a, Case 1) or with disappearance of stained tumor tissue (b, Case 2, arrow). However, some HCCs underwent gradual decreases in size without the disappearance of early staining. In these two cases, HCCs were locally controlled > 3 years after PBT

PBT proton beam therapy, *RECIST* response evaluation criteria in solid tumors, m-RECIST modified RESIST, *EASL* European Association for the Study of the Liver, *RECICL* response evaluation criteria in cancer of the liver by the Liver Cancer Study Group of Japan, *PR* partial response, *CR* complete response, *TE* treatment effect

Several sets of response evaluation criteria are available for estimating the therapeutic effects on tumors. These criteria are as follows: (1) Measuring changes in tumor size (WHO guidelines; Response Evaluation Criteria in Solid Tumors [RECIST]) [53, 54]. (2) Measuring changes in enhancement (European Association for the Study of the Liver [EASL] guidelines) [54, 55]. (3) Measuring changes in tumor enhancement size (Modified RECIST [m-RECIST]) [56, 57]. (4) Measuring tumor necrosis as an unenhanced area in the tumor [Response Evaluation Criteria in Cancer of the Liver by the Liver Cancer Study Group of Japan (RECICL)] guidelines (Fig. 11; Table 2) [58].

These criteria are used for patients with HCC who undergo chemotherapy, transarterial chemoembolization, and percutaneous ablation (percutaneous ethanol injection or radiofrequency). In contrast to these locoregional

treatments, dynamic CT and MRI analyses of HCC after radiation therapy often show gradual decreases in tumor size with preserved arterial blood supply (Fig. 11) [59, 60]. It is important to know that the residual contrast enhancement of CT or MRI used to analyze HCCs does not necessarily indicate a remaining viable tumor [60].

Irradiated HCCs may retain early enhancement and, therefore, RECIST, EASL, m-RECIST, and RECICL miss or underestimate clinically complete and partial remissions of HCCs when assessing the therapeutic efficacy of locoregional radiation therapies. Local control is often assessed using CT and MRI to simply determine if there is incremental tumor enlargement. For example, 93% of viable, treated HCCs show hyperintensity and hypointensity on DWI and ADC maps, respectively. Mean signal intensity ratios and ADC values of viable tumors are significantly higher and lower, respectively, compared with those of irradiated liver. These findings led to the conclusion that adding DWI to conventional MRI is useful for detecting viable HCC tumors treated with radiotherapy compared with conventional MRI alone (Fig. 7) [28]. However, standard criteria that consider this feature are not available for the evaluation of irradiated HCC. Further studies are, therefore, required to establish more accurate post-radiation criteria to assess HCC.

Conclusions

Knowledge of the pathological changes and imaging features of RILD and the changes in the surrounding liver and irradiated regions are important for understanding imaging findings after radiation therapy. Focal liver injury after focal liver irradiation can be visualized during the HBP of EOB-MRI. Caution must be used in monitoring HCC after radiation therapy, because some nonviable lesions retain arterial enhancement. DWI may be helpful in these cases, although further study is required to evaluate therapeutic effects.

Acknowledgements This paper was presented at the 102nd annual meeting of the Radiological Society of North America (RSNA) in Chicago, 2016. It received a Certificated of Merit for an education exhibit. The authors wish to acknowledge Dr. Kazusi Kishi, MD, PhD, Hokkaido Ohno Memorial Hospital for his help for editing this paper. This work was supported by JSPS KAKENHI (Grants-in-Aid for Scientific Research) Grant number 16K10273.

Compliance with ethical standards

Conflict of interest The authors declare that they have no conflict of interest.

References

1. Reed GB, Cox AJ. The human liver after radiation injury. A form of veno-occlusive disease. Am J Pathol. 1966;48:597–611.
2. Benson R, Madan R, Kilambi R, Chander S. Radiation induced liver disease: a clinical update. J Egypt Natl Canc Inst. 2016;28:7–11.
3. Kalogeridi MA, Zygogianni A, Kyrgias G, Kouvaris J, Chatziioannou S, Kelekis N, et al. Role of radiotherapy in the management of hepatocellular carcinoma: a systematic review. World J Hepatol. 2015;7:101–12.
4. Sharma H. Role of external beam radiation therapy in management of hepatocellular carcinoma. J Clin Exp Hepatol. 2014;4:S122–5.
5. Olsen CC, Welsh J, Kavanagh BD, Franklin W, McCarter M, Cardenes HR, et al. Microscopic and macroscopic tumor and parenchymal effects of liver stereotactic body radiotherapy. Int J Radiat Oncol Biol Phys. 2009;73:1414–24.
6. Herfarth KK, Hof H, Bahner ML, Lohr F, Höss A, van Kaick G, et al. Assessment of focal liver reaction by multiphasic CT after stereotactic single-dose radiotherapy of liver tumors. Int J Radiat Oncol Biol Phys. 2003;57:444–51.
7. Sanuki N, Takeda A, Oku Y, Eriguchi T, Nishimura S, Aoki Y, et al. Influence of liver toxicities on prognosis after stereotactic body radiation therapy for hepatocellular carcinoma. Hepatol Res. 2015;45:540–7.
8. Guha C, Kavanagh BD. Hepatic radiation toxicity: avoidance and amelioration. Semin Radiat Oncol. 2011;21:256–63.
9. Chapman Tobias R, Kumarapeli Asangi R, Nyflot Matthew J, et al. Functional imaging of radiation liver injury in a liver metastasis patient: imaging and pathologic correlation. J Gastrointest Oncol. 2015;6:E44–7.
10. Lawrence TS, Robertson JM, Anscher MS, Jirtle RL, Ensminger WD, Fajardo LF. Hepatic toxicity resulting from cancer treatment. Int J Radiat Oncol Biol Phys. 1995;31:1237–48.
11. Kim TH, Kim DY, Park JW, Kim SH, Choi JI, Kim HB, et al. Dose-volumetric parameters predicting radiation-induced hepatic toxicity in unresectable hepatocellular carcinoma patients treated with three-dimensional conformal radiotherapy. Int J Radiat Oncol Biol Phys. 2007;67:225–31.
12. Cheng JC, Wu JK, Huang CM, Liu HS, Huang DY, Cheng SH, et al. Radiation-induced liver disease after three-dimensional conformal radiotherapy for patients with hepatocellular carcinoma: dosimetric analysis and implication. Int J Radiat Oncol Biol Phys. 2002;54:156–62.
13. Xu ZY, Liang SX, Zhu J, Zhu XD, Zhao JD, Lu HJ, et al. Prediction of radiation-induced liver disease by Lyman normal-tissue complication probability model in three-dimensional conformal radiation therapy for primary liver carcinoma. Int J Radiat Oncol Biol Phys. 2006;65:189–95.
14. U.S. Department of Health and Human Services, National Institutes of Health National Cancer Institute. Common Terminology Criteria for Adverse Events v4.0. https://ctep.cancer.gov/protocolDevelopment/electronic_applications/ctc.htm#ctc_40.
15. Sempoux C, Horsmans Y, Geubel A, Fraikin J, Van Beers BE, Gigot JF, et al. Severe radiation-induced liver disease following localized radiation therapy for biliopancreatic carcinoma: activation of hepatic stellate cells as an early event. Hepatology. 1997;26:128–34.
16. da Silveira EB, Jeffers L, Schiff ER. Diagnostic laparoscopy in radiation-induced liver disease. Gastrointest Endosc. 2002;55:432–4.

VOD path article

17. Anscher MS, Crocker IR, Jirtle RL. Transforming growth factor-beta 1 expression in irradiated liver. Radiat Res. 1990;122:77–85.
18. Liu Y, Shi C, Cui M, Yang Z, Gan D, Wang Y. Different doses of partial liver irradiation promotes hepatic regeneration in rat. Int J Clin Exp Pathol. 2015;8:6554–9.
19. Clément O, Mühler A, Vexler VS, Rosenau W, Berthezène Y, Kuwatsuru R, et al. Evaluation of radiation-induced liver injury with MR imaging: comparison of hepatocellular and reticuloendothelial contrast agents. Radiology. 1992;185:163–8.
20. Erturk SM, Mortelé KJ, Binkert CA, Glickman JN, Oliva MR, Ros PR, et al. CT features of hepatic venoocclusive disease and hepatic graft-versus-host disease in patients after hematopoietic stem cell transplantation. AJR Am J Roentgenol. 2006;186:1497–501.
21. Itai Y, Murata S, Kurosaki Y. Straight border sign of the liver: spectrum of CT appearances and causes. Radiographics. 1995;15:1089–102.
22. Ohtomo K, Baron RL, Dodd GD 3rd, Federle MP, Miller WJ, Campbell WL, et al. Confluent hepatic fibrosis in advanced cirrhosis: appearance at CT. Radiology. 1993;188:31–5.
23. Jeffrey RB Jr, Moss AA, Quivey JM, Federle MP, Wara WM. CT of radiation-induced hepatic injury. Am J Roentgenol. 1980;135:445–8.
24. Takamatsu S, Yamamoto K, Maeda Y, Kawamura M, Shibata S, Sato Y, et al. Evaluation of focal liver reaction after proton beam therapy for hepatocellular carcinoma examined using Gd-EOB-DTPA enhanced hepatic magnetic resonance imaging. PLoS One. 2016;11:e0167155.
25. Kimura T, Takahashi S, Takahashi I, Nishibuchi I, Doi Y, Kenjo M, et al. The time course of dynamic computed tomographic appearance of radiation injury to the cirrhotic liver following stereotactic body radiation therapy for hepatocellular carcinoma. PLoS One. 2015;10:e0125231.
26. Garra BS, Shawker TH, Chang R, Kaplan K, White RD. The ultrasound appearance of radiation-induced hepatic injury. Correlation with computed tomography and magnetic resonance imaging. J Ultrasound Med. 1988;7:605–9.
27. Yankelevitz DF, Knapp PH, Henschke CI, Nisce L, Yi Y, Cahill P. MR appearance of radiation hepatitis. Clin Imaging. 1992;16:89–92.
28. Park HJ, Kim SH, Jang KM, Lim S, Kang TW, Park HC, et al. Added value of diffusion-weighted MRI for evaluating viable tumor of hepatocellular carcinomas treated with radiotherapy in patients with chronic liver disease. Am J Roentgenol. 2014;202:92–101.
29. Kim YK, Kim CS, Han YM, Park G, Hwang SB, Yu HC. Comparison of gadoxetic acid-enhanced MRI and superparamagnetic iron oxide-enhanced MRI for the detection of hepatocellular carcinoma. Clin Radiol. 2010;65:358–65.
30. Rühl R, Lüdemann L, Czarnecka A, Streitparth F, Seidensticker M, Mohnike K, et al. Radiobiological restrictions and tolerance doses of repeated single-fraction hdr-irradiation of intersecting small liver volumes for recurrent hepatic metastases. Radiat Oncol. 2010;5:44.
31. Ichikawa T, Saito K, Yoshioka N, Tanimoto A, Gokan T, Takehara Y, et al. Detection and characterization of focal liver lesions: a Japanese phase III, multicenter comparison between gadoxetic acid disodium-enhanced magnetic resonance imaging and contrast-enhanced computed tomography predominantly in patients with hepatocellular carcinoma and chronic liver disease. Invest Radiol. 2010;45:133–41.
32. Chen L, Zhang J, Zhang L, Bao J, Liu C, Xia Y, et al. Meta-analysis of gadoxetic acid disodium (Gd-EOB-DTPA)-enhanced magnetic resonance imaging for the detection of liver metastases. PLoS One. 2012;7:e48681.
33. Kitao A, Zen Y, Matsui O, Gabata T, Kobayashi S, Koda W, et al. Hepatocellular carcinoma: signal intensity at gadoxetic acid-enhanced MR Imaging-correlation with molecular transporters and histopathologic features. Radiology. 2010;256:817–26.
34. Nassif A, Jia J, Keiser M, Oswald S, Modess C, Nagel S, et al. Visualization of hepatic uptake transporter function in healthy subjects by using gadoxetic acid-enhanced MR imaging. Radiology. 2012;264:741–50.
35. Vander BS, Libbrecht L, Blokzijl H, Faber KN, Moshage H, Aerts R, et al. Diagnostic and pathogenetic implications of the expression of hepatic transporters in focal lesions occurring in normal liver. J Pathol. 2005;207:471–82.
36. Richter C, Seco J, Hong TS, Duda DG, Bortfeld T. Radiation-induced changes in hepatocyte-specific Gd-EOB-DTPA enhanced MRI: potential mechanism. Med Hypotheses. 2014;83:477–81.
37. Dawson LA, Normolle D, Balter JM, McGinn CJ, Lawrence TS, Ten Haken RK. Analysis of radiation-induced liver disease using the Lyman NTCP model. Int J Radiat Oncol Biol Phys. 2002;53:810–21.
38. Dawson LA, Ten Haken RK. Partial volume tolerance of the liver to radiation. Semin Radiat Oncol. 2005;15:279–83.
39. Xu ZY, Liang SX, Zhu J, Zhu XD, Zhao JD, Lu HJ, et al. Prediction of radiation-induced liver disease by Lyman normal-tissue complication probability model in three-dimensional conformal radiation therapy for primary liver carcinoma. Int J Radiat Oncol Biol Phys. 2006;65:189–95.
40. Liang SX, Zhu XD, Xu ZY, Zhu J, Zhao JD, Lu HJ, et al. Radiation-induced liver disease in three-dimensional conformal radiation therapy for primary liver carcinoma: the risk factors and hepatic radiation tolerance. Int J Radiat Oncol Biol Phys. 2006;65:426–34.
41. Zhu J, Zhu XD, Liang SX, Xu ZY, Zhao JD, Huang QF, et al. Prediction of radiation induced liver disease using artificial neural networks. Jpn J Clin Oncol. 2006;36:783–8.
42. Bentzen SM, Constine LS, Deasy JO, Eisbruch A, Jackson A, Marks LB, et al. Quantitative analyses of normal tissue effects in the clinic (QUANTEC): an introduction to the scientific issues. Int J Radiat Oncol Biol Phys. 2010;76:S3–9.
43. Pan CC, Kavanagh BD, Dawson LA, Li XA, Das SK, Miften M, et al. Radiation-associated liver injury. Int J Radiat Oncol Biol Phys. 2010;76:S94–100.
44. Miyagawa S, Makuuchi M, Kawasaki S, Kakazu T. Criteria for safe hepatic resection. Am J Surg. 1995;169:589–94.
45. Urata K, Kawasaki S, Matsunami H, Hashikura Y, Ikegami T, Ishizone S, et al. Calculation of child and adult standard liver volume for liver transplantation. Hepatology. 1995;21:1317–21.
46. Mizumoto M, Okumura T, Hashimoto T, Fukuda K, Oshiro Y, Fukumitsu N, et al. Evaluation of liver function after proton beam therapy for hepatocellular carcinoma. Int J Radiat Oncol Biol Phys. 2012;82:e529–35.
47. Seidensticker M, Seidensticker R, Mohnike K, Wybranski C, Kalinski T, Luess S, et al. Quantitative in vivo assessment of radiation injury of the liver using Gd-EOB-DTPA enhanced MRI: tolerance dose of small liver volumes. Radiat Oncol. 2011. https://doi.org/10.1186/1748-717X-6-40.
48. Boda-Heggemann J, Attenberger U, Budjan J, Jahnke A, Jahnke L, Vogel L, et al. MRI morphologic alterations after liver SBRT: direct dose correlation with intermodal matching. Strahlenther Onkol. 2016;192:641–8.
49. Doi H, Shiomi H, Masai N, Tatsumi D, Igura T, Imai Y, et al. Threshold doses and prediction of visually apparent liver dysfunction after stereotactic body radiation therapy in cirrhotic and normal livers using magnetic resonance imaging. J Radiat Res. 2016;57:294–300.

50. Sanuki N, Takeda A, Oku Y, Eriguchi T, Nishimura S, Aoki Y, et al. Threshold doses for focal liver reaction after stereotactic ablative body radiation therapy for small hepatocellular carcinoma depend on liver function: evaluation on magnetic resonance imaging with Gd-EOB-DTPA. Int J Radiat Oncol Biol Phys. 2014;88:306–11.
51. Nakamura Y, Kimura T, Higaki T, Honda Y, Komoto D, Yamagami T, et al. Clinical utility of gadoxetate disodium-enhanced hepatic MRI for stereotactic body radiotherapy of hepatocellular carcinoma. Jpn J Radiol. 2015;33:627–35.
52. Onaya H, Itai Y, Ahmadi T, Yoshioka H, Okumura T, Akine Y, et al. Recurrent hepatocellular carcinoma versus radiation-induced hepatic injury: differential diagnosis with MR imaging. Magn Reson Imaging. 2001;19:41–6.
53. World health organization, reporting of response, WHO handbook for reporting results of cancer treatment, Genova: World Health Organization Offset Publication; 1979, pp. 22–27.
54. Therasse P, Arbuck SG, Eisenhauer EA, Wanders J, Kaplan RS, Rubinstein L, et al. New guidelines to evaluate the response to treatment in solid tumors. J Natl Cancer Inst. 2000;92:205–16.
55. Forner A, Ayuso C, Varela M, Rimola J, Hessheimer AJ, de Lope CR, et al. Evaluation of tumor response after locoregional therapies in hepatocellular carcinoma: are response evaluation criteria in solid tumors reliable? Cancer. 2009;115:616–23.
56. Eisenhauer EA, Therasse P, Bogaerts J, Schwartz LH, Sargent D, Ford R, et al. New response evaluation criteria in solid tumours: revised RECIST guideline (version 1.1). Eur J Cancer. 2009;45:228–47.
57. Lencioni R, Llovet JM. Modified RECIST (mRECIST) assessment for hepatocellular carcinoma. Semin Liver Dis. 2010;30:52–60.
58. Kudo M, Ueshima K, Kubo S, Sakamoto M, Tanaka M, Ikai I, et al. Response evaluation criteria in cancer of the liver (RECICL) (2015 revised version). Hepatol Res. 2016;46:3–9.
59. Ahmadi T, Okumura T, Onaya H, Akine Y, Itai Y. Preservation of hypervascularity in hepatocellular carcinoma after effective proton-beam radiotherapy-CT observation. Clin Radiol. 1999;54:253–6.
60. Kinjo N, Ikeda Y, Taguchi K, Sugimoto R, Maehara S, Tsujita E, et al. Hepatic resection of hepatocellular carcinoma after proton beam therapy: a case report. Hepatol Res. 2016;46:483–8.